Electronic Supplementary Material (ESI) for Chemical Communications.
This journal is © The Royal Society of Chemistry 2020

Site-selective exposure of iron nanoparticles to achieve rapid interface enrichment for heavy metals

Li Su,[a] Jiaxin Ma,[a] Jiancheng Wang,[a] Wan Jiang,[a] Wei-xian Zhang[b] and Jianping Yang[a]*

[a] State Key Laboratory for Modification of Chemical Fibers and Polymer Materials, College of Materials Science and Engineering, Donghua University, Shanghai 201620, China

[b] College of Environmental Science and Engineering, State Key Laboratory of Pollution Control and Resources Reuse, Tongji University, Shanghai 200092, China.

E-mail for corresponding author: jianpingyang@dhu.edu.cn

MATERIALS AND METHODS

Synthesis of Fe_3O_4@PMO Janus nanoparticles

The monodisperse Fe_3O_4 NPs can be synthesized based on an improved hydrothermal synthesis strategy.[45] The prepared Fe_3O_4 NPs were washed by ethanol and deionized water and re-dispersed in ethanol to form a stable solution with a concentration of ~ 25 mg/mL. The preparation of Janus nanoparticles of Fe_3O_4@PMO was based on the Stöber method. 2 mL of the Fe_3O_4 NPs ethanol solution was added into a solution containing 70 mL of deionized water, 4 mL ethanol, 150 mg of Cetyltrimethyl Ammonium Bromide (CTAB, Mackun) and 1.8 mL ammonia aqueous (28 wt %, Sinopharm) by sonication for 15 min and agitation for 30 min. Then, 50 μL of 1,2-Bis(triethoxysilyl)ethane (BTEE, Sigma-Alorich) was added dropwise with continuous stirring, and the mixture proceeded for 3 h. The obtained products (denote as Fe_3O_4@PMO-1 Janus mesoporous nanoparticles) were washed by ethanol and deionized water and collected by centrifugation, and dispersed in ethanol. Based on the above steps, the dose of BTEE was respectively regulated to 100 μL and 200 μL, and the resulting products denoted as Fe_3O_4@PMO-2 and Fe_3O_4@PMO-3. Subsequently, the ratios of H_2O-ethanol were regulated at 60: 14 and 50: 24 when the dose of the BTEE was 100 μL, the resulting products were denoted as Fe_3O_4@PMO-4 and Fe_3O_4@PMO-5.

Synthesis of Fe@PMO Janus nanoparticles

The preparation Fe_3O_4@PMO-X (1, 2, 3, 4, 5) were treated at 600 ℃ for 3 h in 50 %

volume fraction H_2 atmosphere ((the mixture gas of Ar / H_2), with a ramp rate of 1 ℃/ min. Then, the Fe@PMO-X (1, 2, 3, 4, 5) Janus nanoparticles were obtained.

Noble-metal removal from water

Before the noble-metal extraction, the as-prepared Janus Fe@PMO were dispersed in deionized water into uniform dispersion with a catalyst concentration of 50-250 mg/mL. The initial noble-metal-containing solution with 1 mg/L were adjusted with 0.1 M HCl or NaOH at the start of the experiment. Then, 8 mL aqueous solution of Fe@PMO added into 200 mL noble-metal-containing solution without eliminate dissolved oxygen. After a certain interval, 6 mL of the mixed solution was separated by centrifugation and magnetic separation. The concentration of metal ions in the supernatant was determined by inductively coupled plasma (ICP) spectrometer.

Electrochemical test

Tafel test was used detect the electrocatalytic activity between voltage -2.4V to 0.0 V. Two test systems are respectively a solution with a pH of 3, and a solution system with a concentration of 1 mg/L Au(Ⅲ). Subsequently, we regulate the pH values of Fe@PMO-1 and Fe@PMO-3 from 2 to 8 for the Zeta potential test at room temperature. The maximal voltage is 200 mV, and repeat the test three times.

Characterization

The morphological structure was structure was characterized by transmission electron microscopy (TEM, JEM-2100F) and scanning transmission electron microscopy (SEM, Hitachi S-4800). The energy-dispersive X-ray spectroscopy element mapping was performed on a FEI Talos F200S. X-ray diffraction (XRD) patterns were recorded on a

Rigaku D/Max-2550 PC diffractometer (Tokyo, Japan) equipped with Cu Kα radiation. The samples were degassed under vacuum at 100 for 12 h before nitrogen absorption and desorption test used by Quantachrome Atuosorb-iQ. The pore volumes and pore size distributions are analyzed by BJH model and the specific surface areas were calculated by using the BET method.

The chemical equation for the reaction of Fe nanoparticles and hydrogen ions

$$2Fe^{0}_{(s)} + 4H^{+}_{(aq)} + O_{2(aq)} \longrightarrow 2Fe^{2+}_{(aq)} + 2H_2O_{(l)}$$
$$Fe^{0}_{(s)} + 2H_2O_{(aq)} \longrightarrow Fe^{2+}_{(aq)} + H_{2(g)} + 2OH^{-}_{(aq)}$$

The quasi-first-order kinetic model calculation formula

The quasi-first-order kinetic model is shown as follows:[1]

$$\frac{d[U]}{dt} = -K_{obs} \cdot [U]$$

K_{obs} (reaction rate constants): Apparent rate constant of pseudo first order reaction, min^{-1}

[U]：Au(Ⅲ) concentration at reaction time t in solution, mg/L

$[U]_0$：Initial concentration of Au(Ⅲ) in solution, mg/L

t: reaction time, min

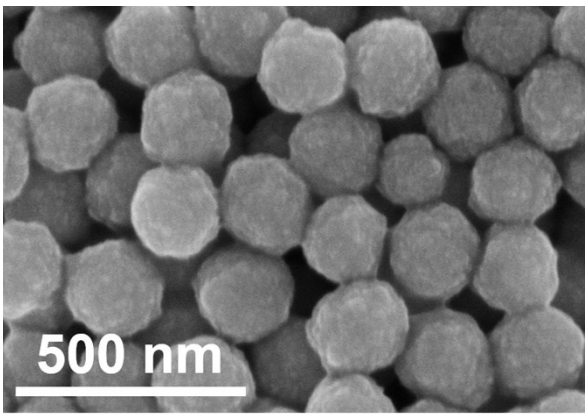

Fig. S1 SEM image of Fe_3O_4 nanoparticles.

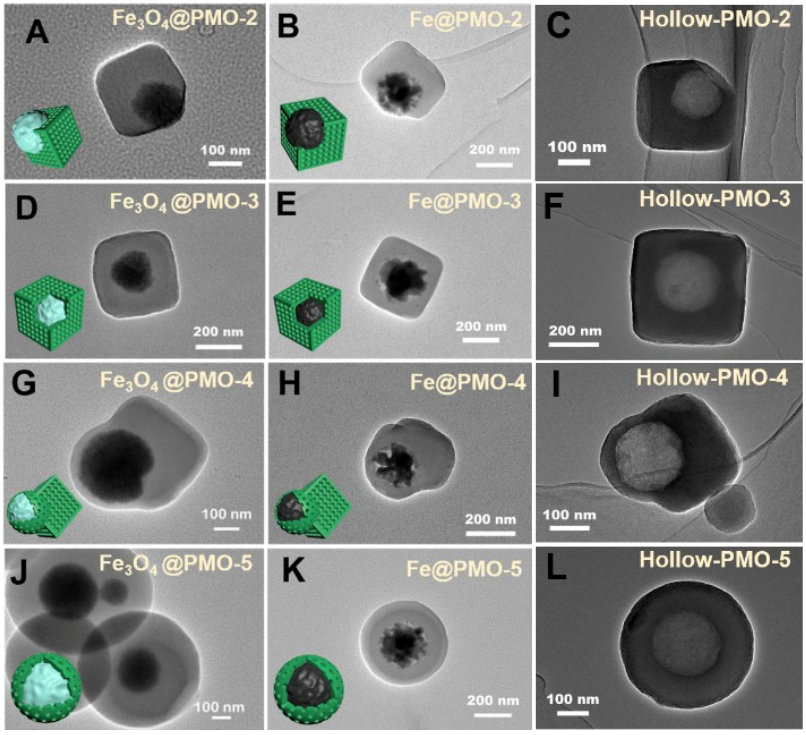

Fig. S2 The TEM images and corresponding images of 3D model images (A) Fe_3O_4@PMO-2, (B) Fe@PMO-2, (D) Fe_3O_4@PMO-3, (E) Fe@PMO-3, (G) Fe_3O_4@PMO-4, (H) Fe@PMO-4, (J) Fe_3O_4@PMO-5, (K) Fe@PMO-5. (C) Hollow-PMO-2, (F) Hollow-PMO-3, (I) Hollow-PMO-4, (L) Hollow-PMO-5 etched by hydrochloric acid.

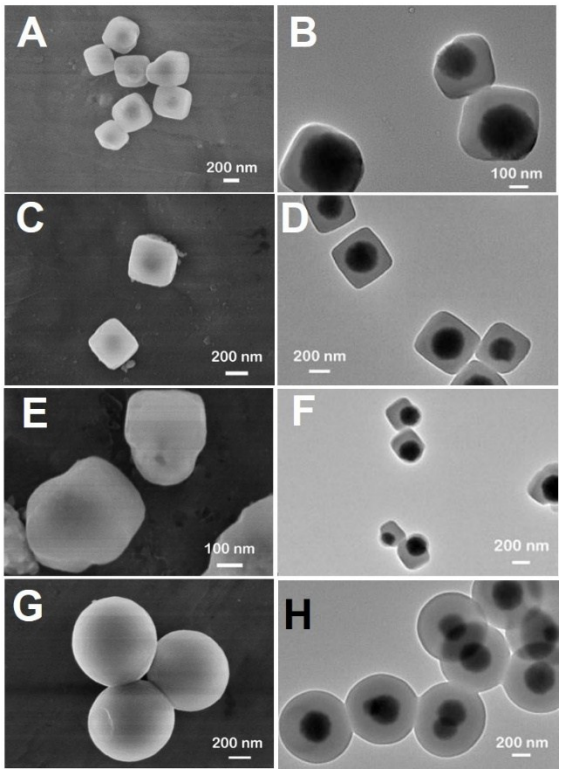

Fig. S3 SEM images and corresponding Low-TEM images, (A) and (B) Fe_3O_4@PMO-2; (C) and (D) Fe_3O_4@PMO-3; (E) and (F) Fe_3O_4@PMO-4 (G) and (H) Fe_3O_4@PMO-5.

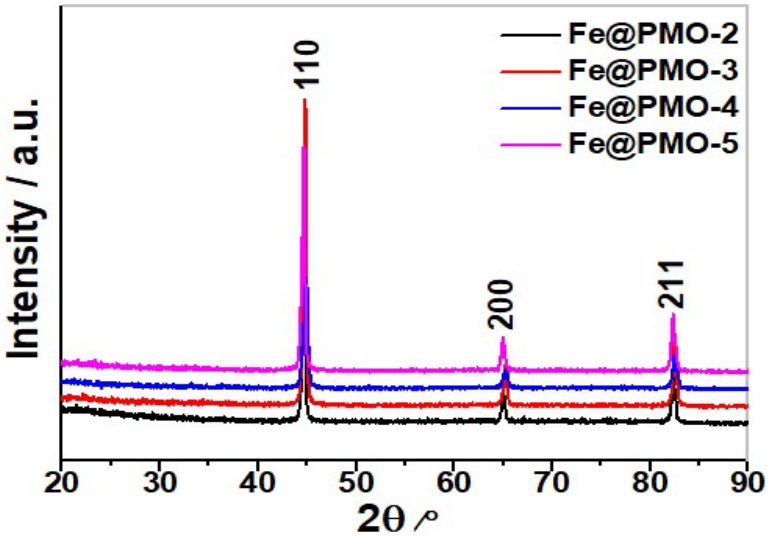

Fig. S4 XRD patterns of the Fe@PMO-X (2, 3, 4, 5) prepared by thermal reduction.

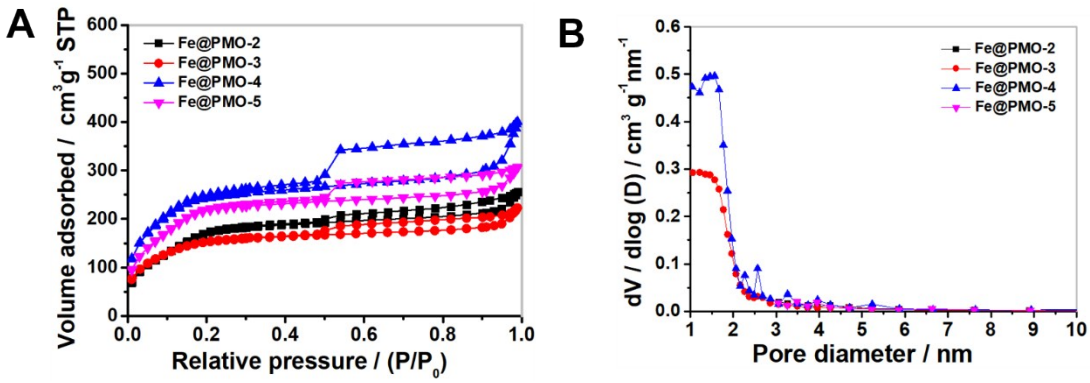

Fig. S5 (A) N_2 adsorption-desorption isotherms of Fe@PMO-X (2, 3, 4, 5), (B) pore size distribution curves.

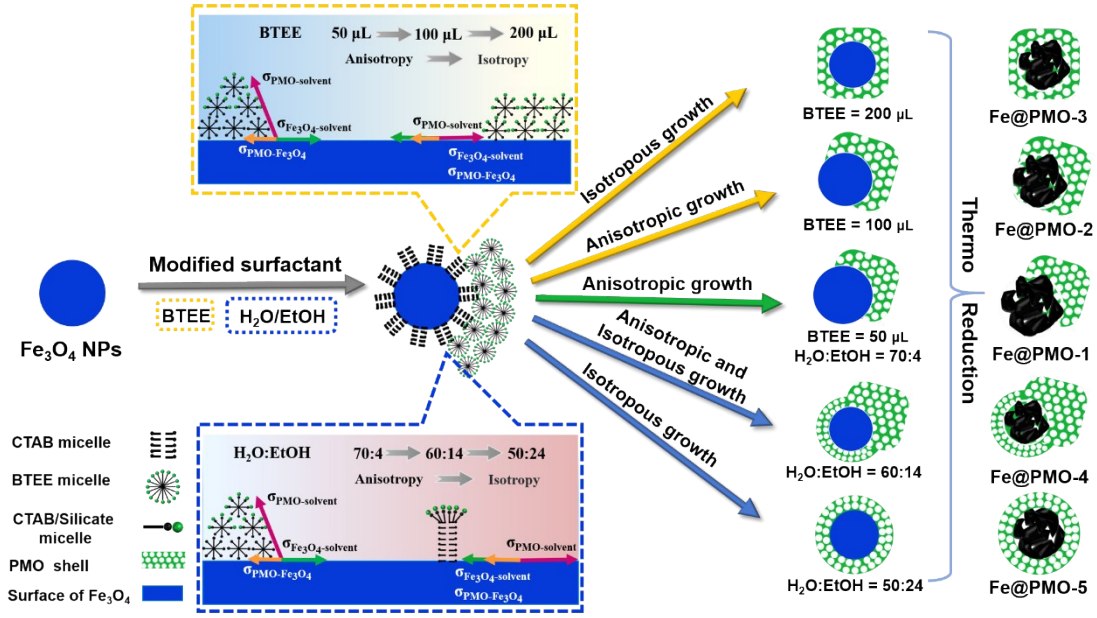

Fig. S6 Schematic diagram evolution of the nucleation and growth mechanism of the CTAB/silicate micelle on the Fe_3O_4 nanoparticles surface to form Fe@PMO derived from Fe_3O_4@PMO with Janus or core-shell nanostructure. The change of chemical environment has little effect on the surface energy of $\sigma_{Fe3O4\text{-}PMO}$.

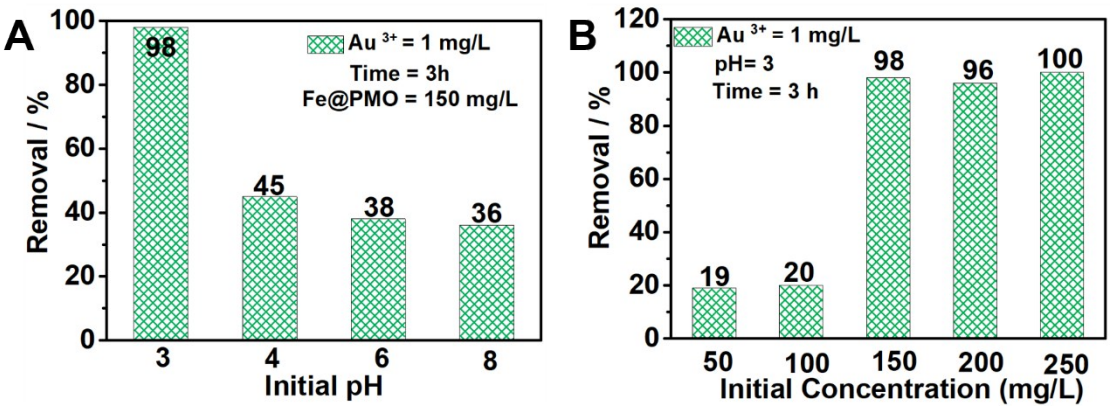

Fig. S7 (A) Au(Ⅲ) removal efficiency of Fe@PMO-l at different pH. (B) Au(Ⅲ) removal capacity of Fe@PMO-l with different concentration.

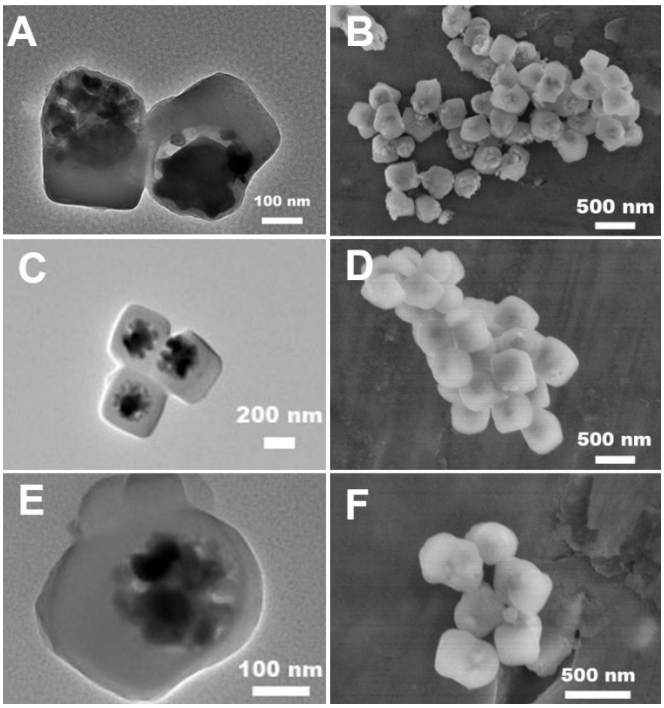

Fig. S8 TEM images and corresponding SEM images of reduction of gold nanoparticles by Fe@PMO (A) and (B) Fe@PMO-Au-1, (C) and (D) Fe@PMO-Au-2, (E) and (F) Fe@PMO-Au-4.

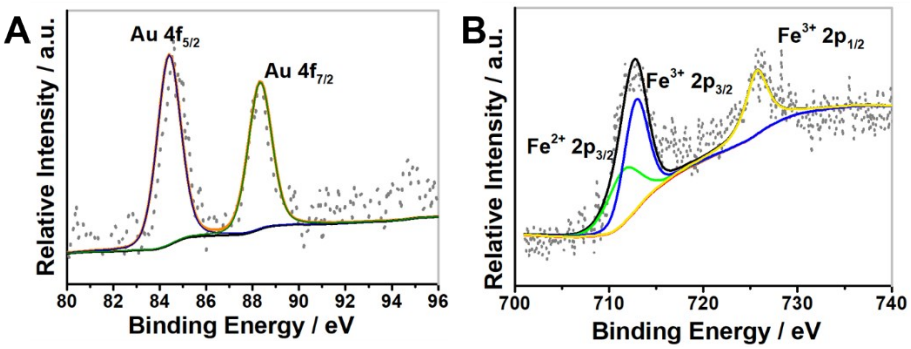

Fig. S9 (A) and (B) the Au 4f and Fe 2p high-resolution XPS spectra of Fe@PMO-Au-1.

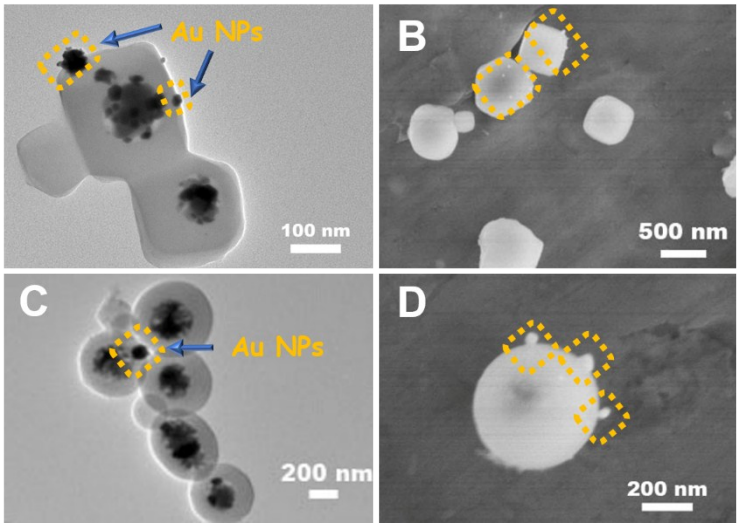

Fig. S10 TEM images and corresponding SEM images of reduction of gold nanoparticles by Fe@PMO (A) and (B) Fe@PMO-Au-3, (C) and (D) Fe@PMO-Au-5.

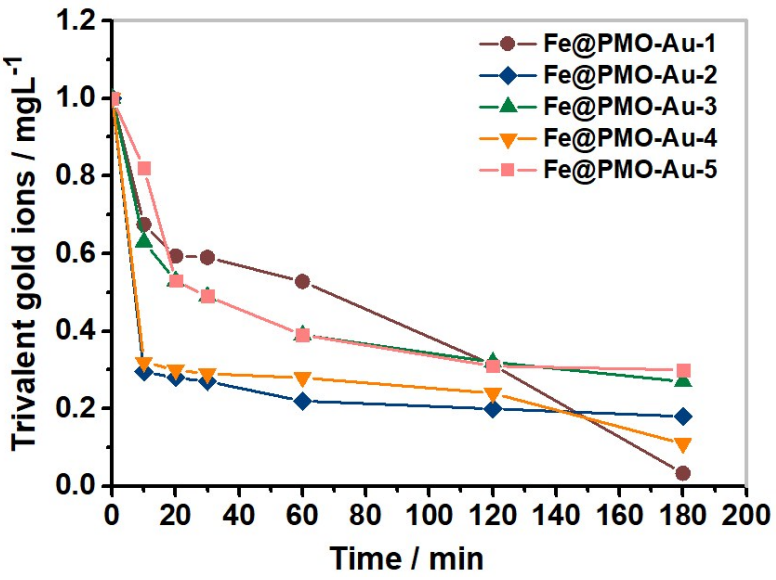

Fig. S11 Kinetics for Au(Ⅲ) removal with Fe@PMO-X (X=1,2,3,4,5) under different reaction time (Fe@PMO 250 mg/L, pH=3).

Table S1 Pseudo-first-order rate constants of Au(Ⅲ) by Fe@PMO-X (X=1,2,3,4,5) under initial reaction 10 min.

	Au(Ⅲ) mg/L	Fe@PMO mg/L	pH	K_{obs} min^{-1}
Fe@PMO-1	1 mg/L	250 mg/L	3	0.041
Fe@PMO-2	1 mg/L	250 mg/L	3	0.12
Fe@PMO-3	1 mg/L	250 mg/L	3	0.046
Fe@PMO-4	1 mg/L	250 mg/L	3	0.114
Fe@PMO-5	1 mg/L	250 mg/L	3	0.019

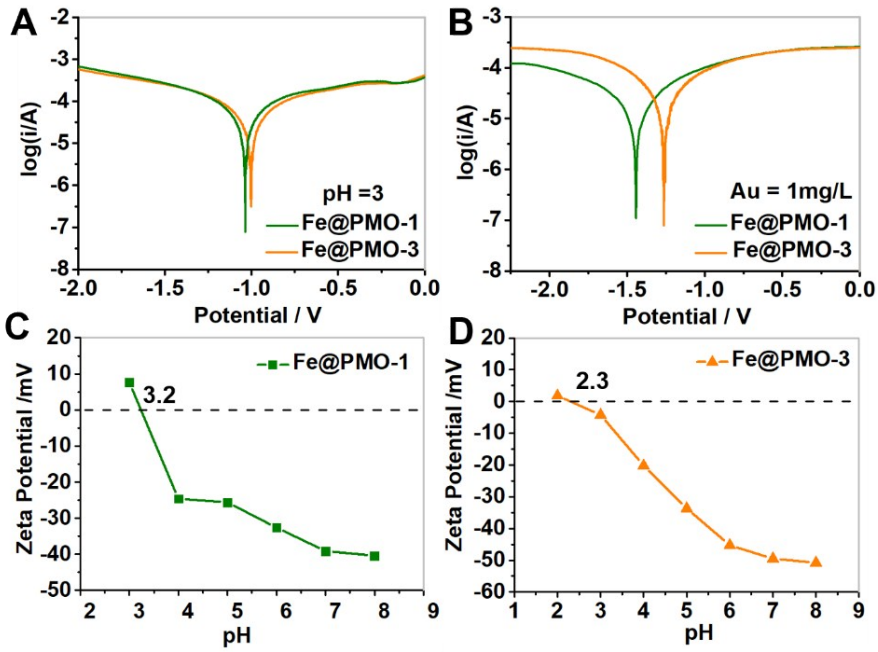

Fig. S12 Polarization curves of Fe@PMO-1and Fe@PMO-3 electrodes (A) a pH =3 system (hydrochloric acid regulation, mercurous sulfate as the reference electrode), (B) Au = 1 mg/L water system (mercury oxide as the reference electrode). Zeta potential of Fe@PMO as a function of solution pH (C) Fe@PMO-1, (D) Fe@PMO-3.

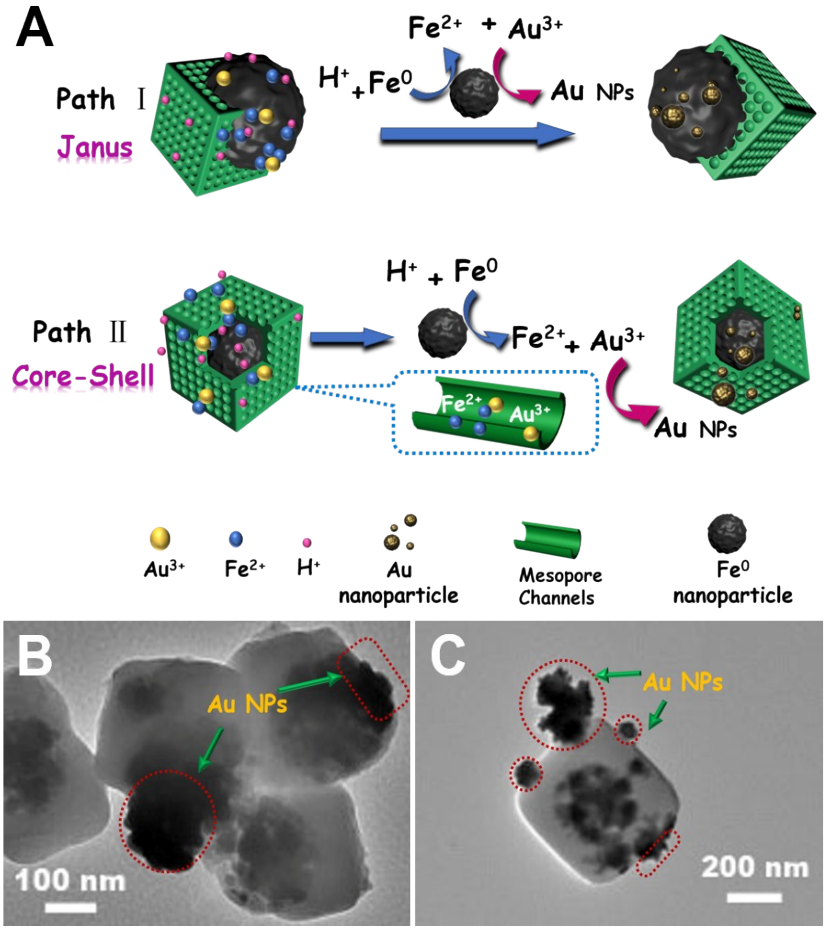

Fig. 13 (A) Schematic diagram of the mechanism of metal ion reduced by Fe@PMO. The TEM of metal ions reduced by Fe@PMO nanoparticles, (B) Fe@PMO-Au-1, (C) Fe@PMO-Au-3.

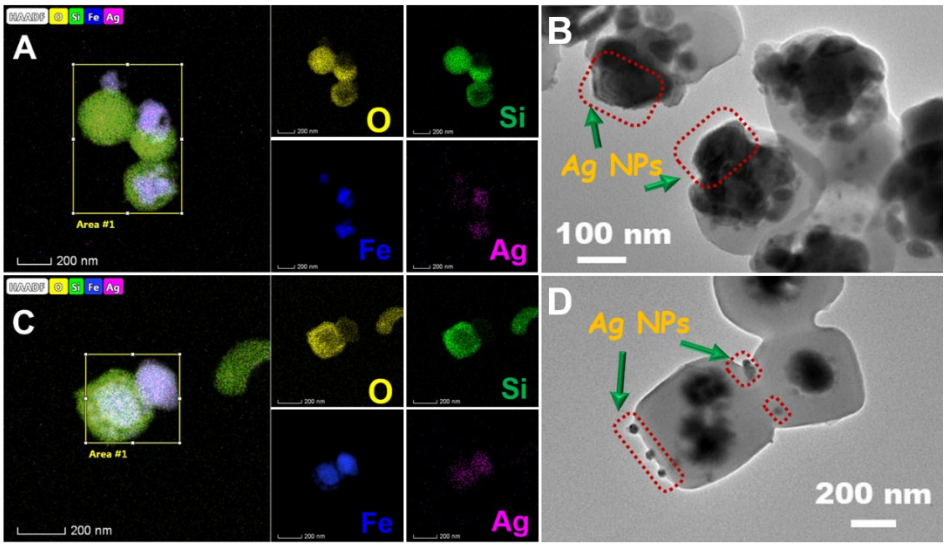

Fig. S14 Dark field TEM image of a single microsphere and the corresponding elemental mapping of (A) Fe@ PMO-Ag-1, (B) Fe@ PMO-Ag-3 for O, Si, Fe and Ag.

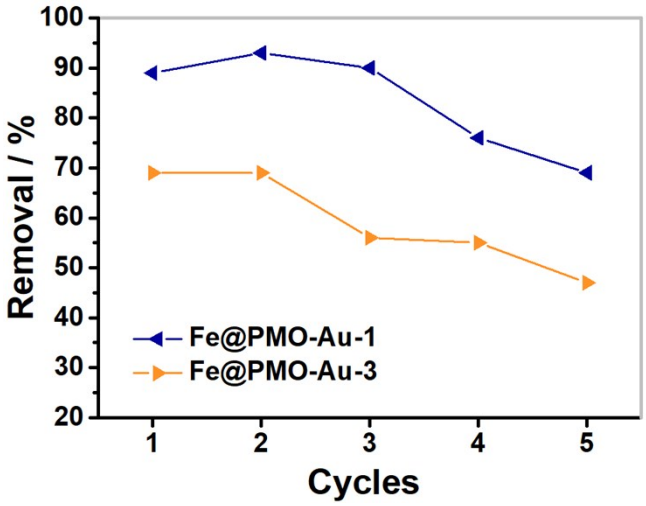

Fig. S15 The Au(Ⅲ) removal of cycles on Fe@PMO-Au-1 and Fe@PMO-Au-3 in 1 mg/L Au(Ⅲ) at 3 h (3 h for one cycle).

Reference

1. Hua, Y. L.; Gu, T. H.; Liu J.; Wang W.; Zhang W. X., *J Environ Sci,* 2018, **67**, 1-3.